

# Chemistry–A European Journal

Supporting Information

## **Atmospheric Ignition Chemistry of Green Hypergolic Bipropellant 1-Ethyl-3-Methylimidazolium Cyanoborohydride – Hydrogen Peroxide in an Acoustic Levigator: Exploring a Potent Universal Propellant**

Souvick Biswas, Mason McAnally, Steven D. Chambreau, Stefan Schneider, Rui Sun, and Ralf I. Kaiser\*

Supporting Information for

**Atmospheric Ignition Chemistry of Green Hypergolic Bipropellant 1-Ethyl-3-Methylimidazolium Cyanoborohydride – Hydrogen Peroxide in an Acoustic Levitator: Exploring a Potent Universal Propellant**

Souvick Biswas<sup>1</sup>, Mason Mcanally<sup>1</sup>, Steven D. Chambreau<sup>2</sup>, Stefan Schneider<sup>2</sup>, Rui Sun<sup>1\*</sup>, Ralf I. Kaiser<sup>1\*</sup>

<sup>1</sup> Department of Chemistry, University of Hawai'i at Manoa, Honolulu, Hawaii 96822, United States

<sup>2</sup> Air Force Research Laboratory, Edwards Air Force Base, California 93524, United States

\* Corresponding authors. E-mail: [ruisun@hawaii.edu](mailto:ruisun@hawaii.edu), [ralfk@hawaii.edu](mailto:ralfk@hawaii.edu)

## **S1. Experimental methods**

**S1.1. Ultrasonic levitator apparatus:** In the acoustic levitator apparatus used in the present experiment, ultrasonic sound waves with a frequency of 58 kHz are produced by a piezoelectric transducer and they are reflected from a concave plate mounted vertically upwards thus generating a standing wave. The soundwaves produce acoustic radiation pressure, which allows a liquid droplet or a tiny solid particle to levitate slightly below one of the pressure minima of the standing wave.<sup>1-3</sup> The distance between the transducer and reflector is set to 2.5 times the wavelength of the soundwave used in the set up (or 14.8 mm) producing five pressure nodes in total, although only the second and third pressure nodes above the ultrasonic transducer are suitable for levitation. The largest diameter of droplets or particles that can be held steadily while levitated in the present apparatus is approximately 3 mm, whereas the smallest could be as low as 15  $\mu\text{m}$ . Here, the droplets loaded in the pressure nodes before merging were oblate spheroidal shaped and their horizontal and vertical diameters measured in the ranges of 1.8-3.0 mm and 1.0-2.1 mm, respectively.

**S1.2. Process chamber and sampling system:** The levitator assembly is enclosed within a pressure-compatible process chamber with a total volume of about 15 liters made of stainless steel to permit levitation in an inert gas or a highly reactive gas to investigate chemical reactions (Figure S1). The process chamber is also surrounded by spectroscopic (FTIR, Raman and UV-Vis spectrometers) as well as visualization tools (high-speed optical and infrared cameras) to identify any characteristic chemical or physical alterations of the levitated sample(s). In the present experiments, the chamber was filled with pure argon and different compositions of argon-molecular oxygen gas mixtures at 298 K with total pressure of 900 Torr. To load chemically distinct droplets in adjacent pressure nodes of the levitator, two syringes are attached to an outside port on the chamber. Each syringe is connected via chemically inert PTFE tubing to one of two microneedles inside the chamber. The pair of needles is attached to the end of a wobble stick. This dual droplet deposition system enables either needle tip to be precisely positioned within the second or third pressure minimum to load a droplet before being withdrawn to a rest position prior to the experiments.

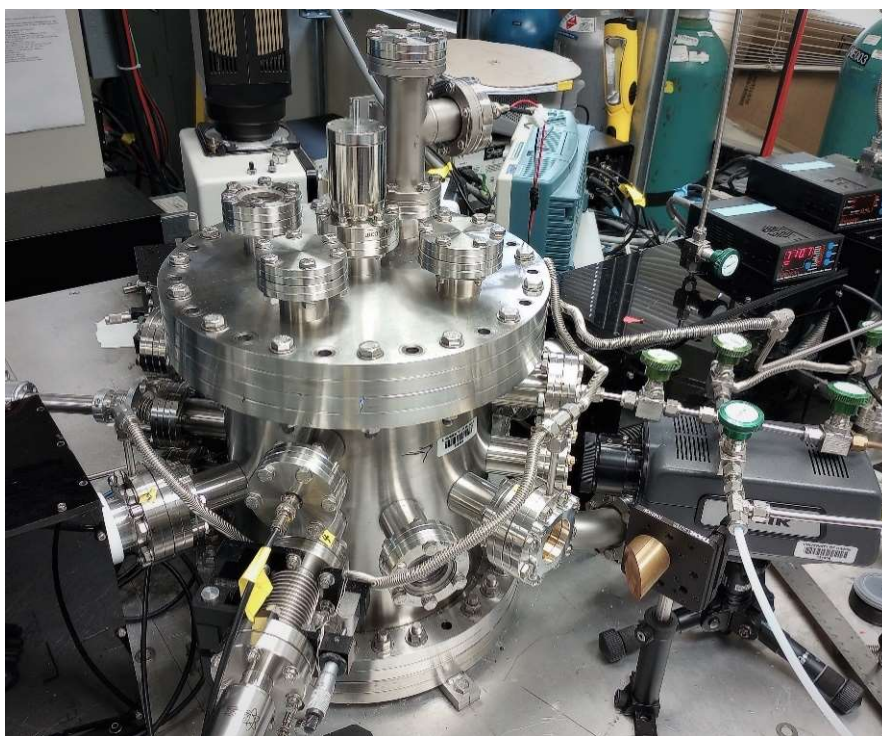


**Figure S1.** Side view of the levitator experimental setup containing the levitation device.

**S1.3. Droplet merging:** First, one droplet of the ionic liquid ([EMIM][CBH]) was loaded in the second pressure minimum above the ultrasonic transducer; hereafter the droplet of the oxidizer, hydrogen peroxide ( $\text{H}_2\text{O}_2$ ) was dispensed into the pressure minimum above. Second, the chirped pulse of 1 s duration with the modulation voltage of typically 600-900 mV was applied to tune in for the resonant frequency (Figure S2). Initially the droplets undergo only non-axisymmetric oscillations, which were not sufficient to de-trap or dislocate them out of the acoustic potential wells. Third, as soon as the resonant frequency for the axial oscillations was attained in the chirp, there occurs a deformation in one of the droplets, making it a prolate spheroid from an oblate one along the vertical axis. The oscillation was further amplified due to the significantly high value of modulation voltage applied. Due to this excitation to the resonant normal mode of the droplet, it initiated vertical oscillation and further merged with the other droplet positioned at the alternate pressure node driven by the surface tension. The merging motion can be initiated in either of the droplets, depending upon the size and mass.<sup>2,4</sup>

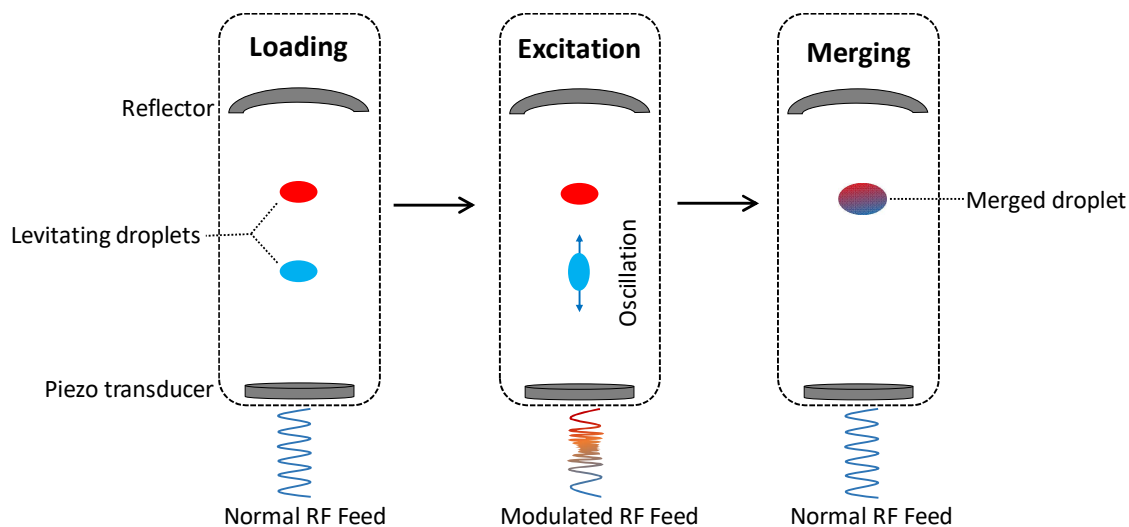


**Figure S2.** Schematic of droplet merging approach in the ultrasonic levitator utilizing an externally triggered chirped pulse in the range of 1-50 Hz to match the modulation frequency.

**S1.4. UV-Vis emission spectroscopy:** In the UV-Vis spectrometer system, the end of a fiber-optic probe is attached to an x, y, z manipulator located inside the process chamber. The manipulator enables the probe to be precisely aligned on the droplets at approximately 10-15 mm. The electromagnetic radiation emitted by the flame upon ignition due to droplet merging is collected by the optical fiber, exits the chamber via a conflat fiber-optic feedthrough, and finally enters a StellarNet SILVER-Nova UV-Vis spectrometer. The spectrometer operates in the 200-1100 nm spectral range with a resolution at full-width half-maximum (fwhm) of 2 nm and is capable of measuring emission spectral traces resulting from flame in a millisecond temporal resolution.

**S1.5. FTIR spectroscopy:** The gases produced by the merging of the droplets followed by ignition were identified by collecting an FTIR absorbance spectrum in the 400-4000  $\text{cm}^{-1}$  wavenumber region through the full width of the process chamber. The FTIR spectrometer system combines a Nicolet 6700 FTIR spectrometer (Thermo Scientific) with two stages of copper mirror optics. The infrared incident beam from the spectrometer was focused into a diameter of 4 mm around the levitated sample before re-collimating prior to detection by a liquid nitrogen cooled MCT-B (mercury cadmium telluride, wide band) detector. The acquisition time for each spectrum was 10 s at a spectral resolution of 4  $\text{cm}^{-1}$  for the instrument. In the experiment, to get the FTIR spectrum for the newly generated gaseous products, first a background spectrum was recorded immediately

after loading the droplets, which was then subtracted from the spectrum acquired after ignition event. The number densities or number of moles of the major gases (for hydrogen cyanide (HCN), carbon dioxide (CO<sub>2</sub>), carbon monoxide (CO) and methane (CH<sub>4</sub>)) evolved during merging events followed by ignition are evaluated from the recorded calibration curves obtained by taking different pressures of the respective gases individually in the process chamber maintaining the identical experimental conditions (Figures S7-S10). Methanol (CH<sub>3</sub>OH) vapor generated in the gas phase is quantified by using the absorption cross-section values for the band centered at 1033 cm<sup>-1</sup>.<sup>5</sup>

**S1.6. The optical and infrared movies and snapshots:** To record high-speed events, a Phantom Miro 3a10 camera operating at repetition rate up to 1 kHz combined with a Navitar Zoom 6000 modular lens system was aligned on the levitated sample via an optical viewport. Infrared thermal imaging videos of the merging events were recorded using an FLIR A6703sc camera. The camera was set to a repetition rate of 250 Hz and the infrared camera was also partially used to determine temperature changes of the levitated droplets while merging. Both optical and IR cameras were triggered externally by the pulse generator synchronized with the UV-Vis spectrometer.

**S1.7. Pulse sequence:** The droplet merging, and the successive ignition event occur at a few milliseconds time regime; therefore, each spectroscopic as well as visual detection methods needed to be synchronized. For this purpose, all the data collection tools except the FTIR spectrometer were synchronized and externally triggered by a pulse generator, (Quantum Composer Plus, model-9518) operating at 1 kHz repetition rate. A schematic of the typical pulse sequencing is depicted in Figure S3. The merging-up chirp, which was generated by the waveform/function generator was triggered in a single-shot mode, spanning 1 s. The UV-Vis spectrometer to detect the intermediate species formed during the ignition was also triggered in single-shot mode with a typical delay of 100 ms since trigger (T<sub>0</sub>), enabled to capture 127 consecutive spectral traces with a temporal resolution of 2 ms. On the other hand, the optical and infrared camera were operated in burst mode which implies the number of pulses were limited to a certain value. As the infrared camera was only capable of operating up to one-fourth of the trigger repetition rate, it was synchronized by providing 3 milliseconds wait time with respect to T<sub>0</sub>, which captured thermal images every fourth pulse from T<sub>0</sub>, thus, it was synchronized with the optical video frames.

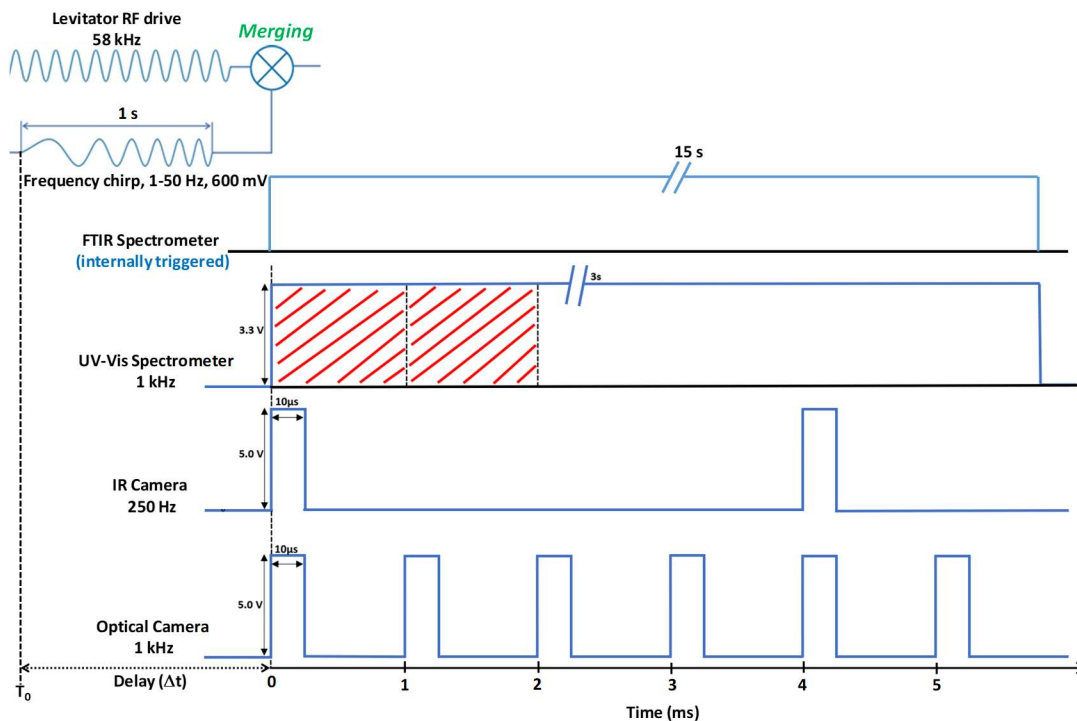


**Figure S3.** Typical pulse sequence used for operation of the ultrasonic levitator, droplet merging and data recording.

## S2. Enrichment of H<sub>2</sub>O<sub>2</sub>

Vacuum distillation of 30% H<sub>2</sub>O<sub>2</sub> was performed to reach concentrated H<sub>2</sub>O<sub>2</sub> (> 90%).<sup>6</sup> A pump was attached to maintain a sufficient pressure gradient throughout the distillation process. All of the glassware were properly cleaned with acid solution (sulfuric acid) and rinsed with dilute (3%) H<sub>2</sub>O<sub>2</sub> before use. To obtain a concentration of ~ 90% H<sub>2</sub>O<sub>2</sub> starting from a concentration of 30%, multiple rounds of distillation were performed by stepwise removal of wastewater. Each cycle takes around 2-3 hours. A quantity of 40 ml of H<sub>2</sub>O<sub>2</sub> of 30% concentration was introduced into the 100 ml volume glass flask. The heating nest maintained the heating temperature constant (approximately 74 - 77°C) throughout the distillation process.

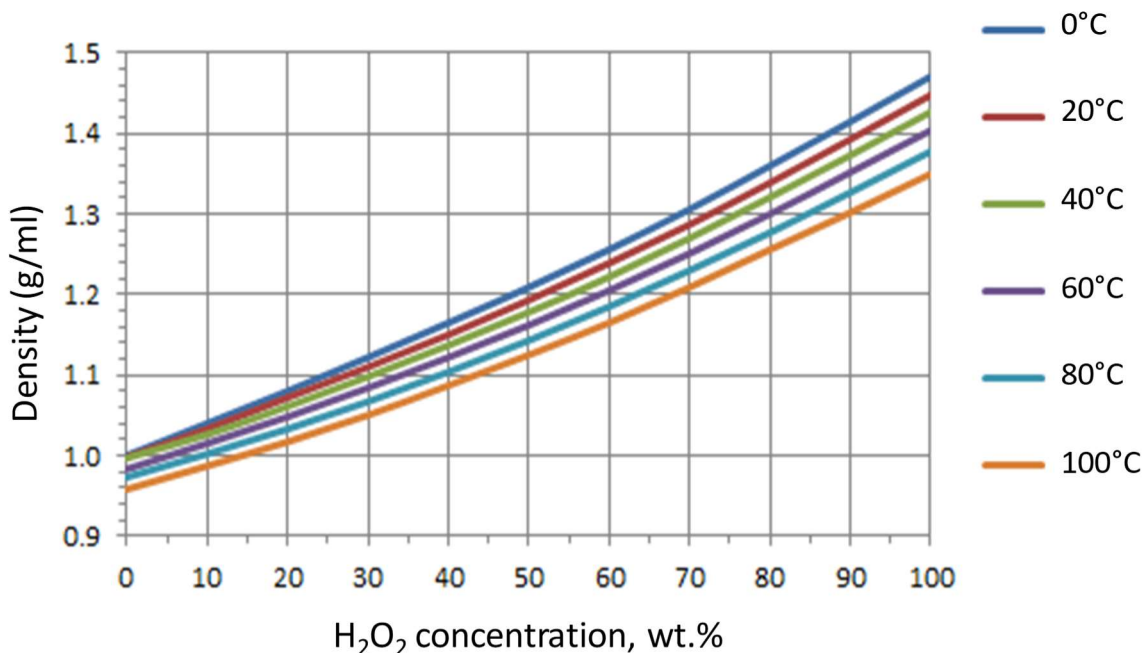


**Figure S4:** Concentration of the hydrogen peroxide as a function of density<sup>7</sup>

At the beginning of the process, the temperature was increased by 1.2°C/min and the heating rate of the oven remained constant after reaching the set temperature. When the mentioned temperature was reached, due to the pressure gradient, water vapor is eliminated and moved through the columns with glass cylinders. Water vapor got condensed on the surface of the interior walls of the cold-water flow and was collected in the 100 ml volume glass flask. The remaining concentrated H<sub>2</sub>O<sub>2</sub> volume ~ 10 ml. Looking at the characteristic specific gravity value (Figure S4) (1.392 g/ml at 20°C for 90% H<sub>2</sub>O<sub>2</sub>), distillation was repeated as per requirement. H<sub>2</sub>O<sub>2</sub> thus obtained was stored in the glass vial (Teflon cap) having at least 40% of empty space. Small, clean glass specific gravity bottles were used to determine density with respect to distilled water. After repeated distillation procedures, the concentration of the resultant H<sub>2</sub>O<sub>2</sub> achieved was 1.401 g/ml, which corresponds to aqueous solution of 92.3 ± 0.2 % (w/v) of H<sub>2</sub>O<sub>2</sub> (Figure S4). The concentration versus density plot was validated by considering standard H<sub>2</sub>O<sub>2</sub> aqueous solutions of 30, 40 and 50% w/v. However, popular titrimetric methods (e.g. with acidic potassium permanganate solution) are suitable for dilute H<sub>2</sub>O<sub>2</sub> solutions only, and dilution of the enriched H<sub>2</sub>O<sub>2</sub> (> 90 %) can incur large errors due to thermal decomposition of the species – hence, the

titrimetric methods are avoided for the evaluation of concentrated H<sub>2</sub>O<sub>2</sub> strength. In addition, the uncertainty in the determined concentrations from the density curve was within permissible limit.

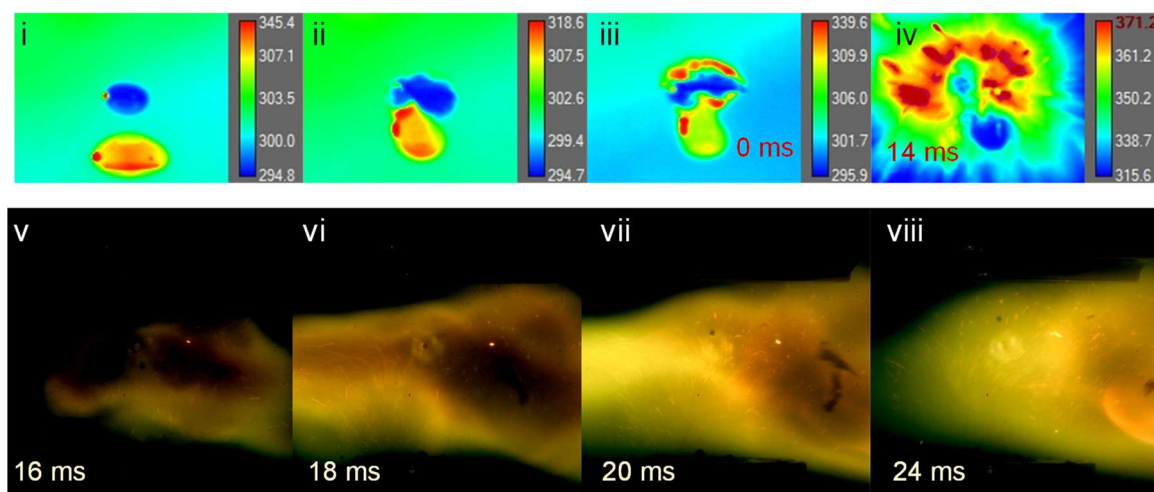


**Figure S5:** Synchronized, temporally resolved complementary infrared and optical camera images of the droplet merging event followed by ignition between [EMIM][CBH] and 92% w/v H<sub>2</sub>O<sub>2</sub> in simulated atmosphere (mixture of 10% O<sub>2</sub> and 90% Ar by volume).

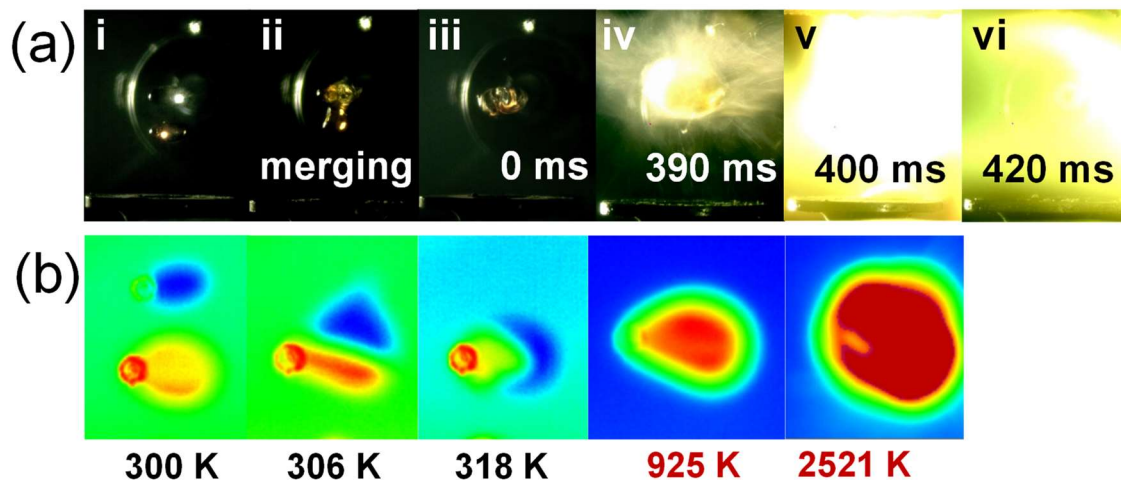


**Figure S6:** Synchronized, temporally resolved complementary (a) optical and (b) infrared camera images of the droplet merging event followed by ignition between [EMIM][CBH] and 92% w/v H<sub>2</sub>O<sub>2</sub> in 100% Ar environment.

### S3. Flame temperature

The relative intensities of the two atomic emission lines (say from  $m$  and  $n$  state) incorporating the Boltzmann population distribution can be expressed as-

$$\frac{I_n}{I_m} = \frac{A_n g_n \nu_n}{A_m g_m \nu_m} \exp[-(E_n - E_m)/kT] \quad (\text{Eq. S1})$$

Where, for  $m$  and  $n$ -states:  $A_m, A_n$  are the emission transition probabilities of the radiation ( $\text{s}^{-1}$ );  $g_m, g_n$  are the statistical weights of the respective levels [=  $(2J + 1)$ ,  $J$  represents the total electronic angular momentum];  $(A_m g_m), (A_n g_n)$  are the weighted transition probabilities ( $\text{s}^{-1}$ );  $\nu_m, \nu_n$  are the emission frequencies ( $\text{cm}^{-1}$ );  $E_m, E_n$  are the absolute energies ( $\text{cm}^{-1}$ ); respectively and  $k$  is Boltzmann constant. If the abovementioned parameters are known,<sup>8</sup> then utilizing the relative intensity ratio of the two atomic emission lines, temperature of the flame,  $T$  can be determined.

In this work, two emission lines of sodium (Na) have been considered to estimate the flame temperature, which are located at 589 (3p→3s) and 819.5 nm (3d→3p). The required parameters have been adopted from the NIST Atomic Spectra Database.<sup>8</sup> The weighted transition probabilities used for 589 and 819.5 nm bands are  $2.46 \times 10^8$  and  $3.08 \times 10^8 \text{ s}^{-1}$ , respectively.

**Table S1.** Mean droplet sizes, number of moles and molar ratios of the reactants for different experimental sets. The errors originate from the volume measurement of the levitating oblate spheroid droplets.

Percentage of O <sub>2</sub>	Mean volume of H <sub>2</sub> O <sub>2</sub> droplet (μl)	Number of moles for H <sub>2</sub> O <sub>2</sub> (× 10 <sup>-5</sup> )	Mean volume of [EMIM][CBH] droplet (μl)	Number of moles for [EMIM][CBH] (× 10 <sup>-5</sup> )	Molar ratio [EMIM][CBH]: H <sub>2</sub> O <sub>2</sub>
0 %	9.1 ± 4.0	34.8 ± 15.3	11.4 ± 4.6	7.2 ± 2.9	1 : 4.8 ± 1.8
10 %	9.6 ± 4.6	36.7 ± 17.6	12.7 ± 4.4	8.0 ± 2.8	1 : 4.6 ± 2.2
20 %	10.1 ± 4.8	38.6 ± 18.3	13.9 ± 4.9	8.7 ± 3.1	1 : 4.4 ± 2.5

**Table S2.** Assignments of the infrared spectral bands of the gas phase products for the reaction of [EMIM][CBH] – H<sub>2</sub>O<sub>2</sub> bipropellant pair at different molecular oxygen concentrations. The literature wavenumbers of the respective band centers are mentioned in parentheses.<sup>9</sup>

Experimental wavenumber (cm <sup>-1</sup> )	Literature wavenumber (cm <sup>-1</sup> )	Carrier	Vibrational mode
3950 - 3490	3950 - 3510 (3657)	H <sub>2</sub> O	O-H stretching
3765 - 3685 3660 - 3580	3760 - 3690 3660 - 3570	CO <sub>2</sub>	O-C-O asymmetric stretching + Fermi doublet of O-C-O symmetric stretching and bending
3770 - 3570	3770 - 3570 (3681)	CH <sub>3</sub> OH	O-H stretching
3880 - 3280	3900 - 3300 (3444), (3337)	NH <sub>3</sub>	N-H asymmetric stretching, N-H symmetric stretching
3400 - 3210	3390 - 3230 (3311)	HCN	C-H stretching
3150 - 2870	3150 - 2880 (3019), (2917)	CH <sub>4</sub>	$\nu_3$ C-H stretching, $\nu_1$ symmetric C-H stretching
3100 - 2770	3150 - 2720 (2999), (2844)	CH <sub>3</sub> OH	C-H perpendicular asymmetric stretching (A') C-H parallel symmetric stretching (A')
2390 - 2300	2385 - 2300 (2349)	CO <sub>2</sub>	O-C-O asymmetric stretching
2300 - 2220	2310 - 2220 (2269)	HNCO	C=N, C=O asymmetric stretching
2220 - 2030	2230 - 2040 (2143)	CO	C-O stretching
1910 - 1320	1900 - 1320 (1595)	H <sub>2</sub> O	H-O-H bending
1510 - 1330	1500 - 1320 (1412)	HCN	1 <sup>st</sup> overtone of bending
1360-1210	1370 -1210 (1306)	CH <sub>4</sub>	$\nu_4$ deformation
1085 - 970	1090 - 960 (1033)	CH <sub>3</sub> OH	C-O stretching (A')
1070 - 840	1120 - 850 (950)	NH <sub>3</sub>	$\nu_2$ deformation (N-H wagging)
780 - 630	790 - 630 (712)	HCN	bending
750 - 630	760 - 630 (667)	CO <sub>2</sub>	bending

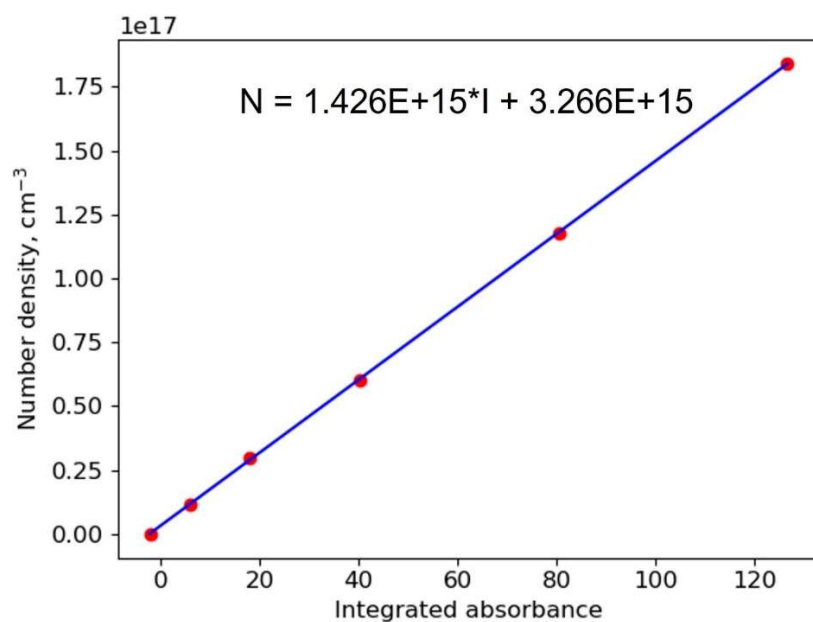


**Figure S7.** Calibration of FTIR signal for hydrogen cyanide (HCN). Integrated area for the CH stretch band in the 3280-3430 cm<sup>-1</sup> range was used.

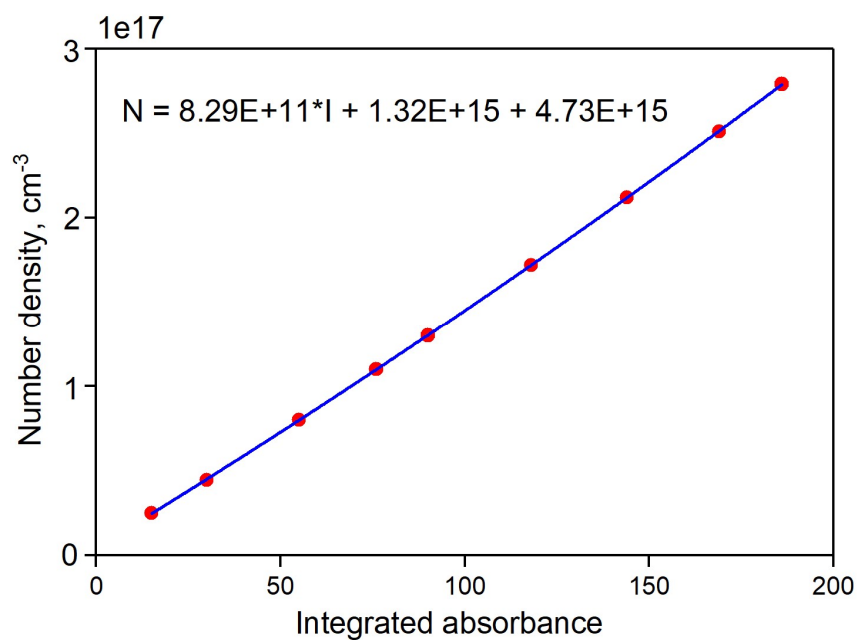


**Figure S8.** Calibration of FTIR signal for carbon monoxide (CO). Integrated area for the CO stretch band in the 2050-2220 cm<sup>-1</sup> range was used.

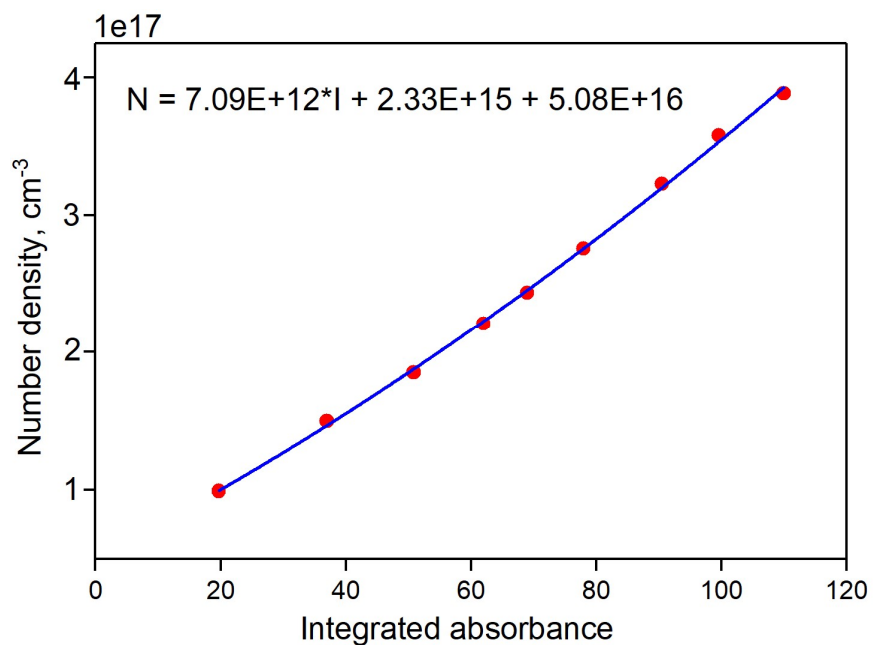


**Figure S9.** Calibration of FTIR signal for methane (CH<sub>4</sub>). Integrated area for the CH stretch band in the 2860-3170 cm<sup>-1</sup> range was used.

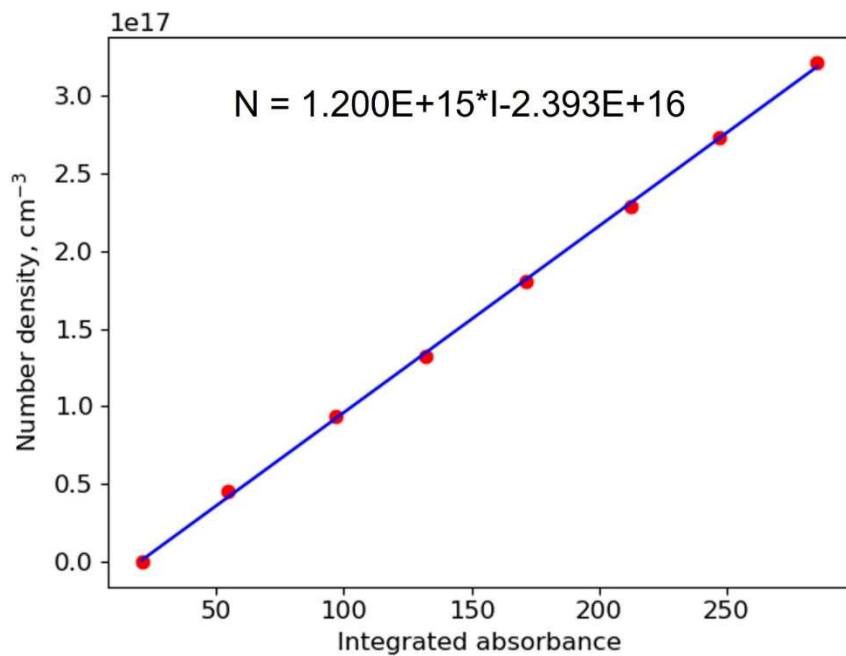


**Figure S10.** Calibration of FTIR signal for carbon dioxide (CO<sub>2</sub>). Integrated area for the CO<sub>2</sub> antisymmetric stretch band in the 2170-2460 cm<sup>-1</sup> range was used.

**Table S3.** Percentage yield of carbon dioxide (CO<sub>2</sub>) from the [EMIM]<sup>+</sup> cation during the reaction. The errors in the number of moles of the [EMIM]<sup>+</sup> and H<sub>2</sub>O<sub>2</sub> originate from the volume measurement errors of the droplets. The errors in number of moles of CO<sub>2</sub> is consisted of the uncertainties in the FTIR measurements and calibration curves.

Percentage of O <sub>2</sub>	Number of moles for H <sub>2</sub> O <sub>2</sub> ( $\times 10^{-5}$ )	Number of moles for [EMIM] <sup>+</sup> ( $\times 10^{-5}$ )	Number of moles of CO <sub>2</sub> ( $\times 10^{-5}$ )	Percentage yield from [EMIM] <sup>+</sup>
0 %	34.8 ± 15.3	7.2 ± 2.9	25.7 ± 3.6	59.5 ± 6.4
10 %	36.7 ± 17.6	8.0 ± 2.8	36.6 ± 4.1	76.1 ± 6.8
20 %	38.6 ± 18.3	8.8 ± 3.1	46.2 ± 4.4	87.8 ± 7.2

**Table S4.** Enthalpy changes of the reactant droplets- ionic liquid ([EMIM][CBH]) and oxidizer (H<sub>2</sub>O<sub>2</sub>) during merging. The resultant specific heat capacity of the liquid mixture was evaluated using the specific heat capacity values for similar type of ionic liquids containing [EMIM]<sup>+</sup> (2.0 Jg<sup>-1</sup>K<sup>-1</sup>) and that of 92% H<sub>2</sub>O<sub>2</sub> (2.69 Jg<sup>-1</sup>K<sup>-1</sup>). The errors in the number of moles and masses originate from the volume measurement errors of the levitating oblate spheroid droplets.

Percentage of O <sub>2</sub>	Mass of [EMIM][CBH] droplet (kg) ( $\times 10^{-6}$ )	Number of moles for [EMIM][CBH] ( $\times 10^{-5}$ )	Mass of H <sub>2</sub> O <sub>2</sub> droplet (kg) ( $\times 10^{-6}$ )	Number of moles for H <sub>2</sub> O <sub>2</sub> ( $\times 10^{-5}$ )	Molar enthalpy change (kJ mol <sup>-1</sup> )
0 %	10.9 ± 4.4	7.2 ± 2.9	12.9 ± 5.6	34.8 ± 15.3	10.9 ± 4.6
10 %	12.1 ± 4.2	8.0 ± 2.8	13.6 ± 6.5	36.7 ± 17.6	15.2 ± 4.9
20 %	13.2 ± 4.7	8.8 ± 3.1	14.3 ± 6.8	38.6 ± 18.3	18.1 ± 5.6

### Supplementary References:

- [1] S. J. Brotton, R. I. Kaiser *Rev. Sci. Instrum.* **2013**, *84*, 055114.
- [2] S. Biswas, I. Antonov, K. Fujioka, G. L. Rizzo, S. D. Chambreau, S. Schneider, R. Sun, R. I. Kaiser *Phys. Chem. Chem. Phys.* **2023**, *25*, 6602-6625.
- [3] S. J. Brotton, R. I. Kaiser *Anal. Chem.* **2020**, *92*, 8371-8377.
- [4] S. Biswas, K. Fujioka, I. Antonov, G. L. Rizzo, S. D. Chambreau, S. Schneider, R. Sun, R. I. Kaiser *Chem. Sci.* **2024**, *15*, 1480-1487.
- [5] J. J. Harrison, N. D. C. Allen, P. F. Bernath *J. Quant. Spectrosc. Radiat. Transf.* **2012**, *113*, 2189-2196.
- [6] C. S. George Pelin, C.-E. Pelin, R. Balasa *INCAS BULLETIN.* **2020**, *12*, 151-157.
- [7] M. F. Easton, A. G. Mitchell, W. F. K. Wynne-Jones *Trans. Faraday Soc.* **1952**, *48*, 796-801.
- [8] A. Kramida, Y. Ralchenko, J. Reader, and NIST ASD Team (2022). NIST Atomic Spectra Database (version 5.10), *National Institute of Standards and Technology, Gaithersburg, MD.* <https://dx.doi.org/10.18434/T4W30F>. (accessed November 4, 2023).
- [9] G. Socrates *Infrared and Raman characteristic group frequencies: tables and charts*, **2001**.